Editors' Suggestion   Featured in Physics

Generalized Scaling and Model for Friction in Wall Turbulence

Shivsai Ajit Dixit,* Abhishek Gupta, Harish Choudhary, and Thara Prabhakaran
Indian Institute of Tropical Meteorology (Ministry of Earth Sciences, New Delhi), Pune, India

(Received 2 May 2023; accepted 22 November 2023; published 2 January 2024)

We present a novel generalized scaling framework and predictive model for wall friction in turbulent flows. The scaling is derived from the dynamical equations, and total mean-flow kinetic energy and the velocity profile shape factor are used as surrogates for dynamical and boundary condition effects. Veracity of the present approach is assessed using data from the literature spanning unprecedented ranges of flow types, Reynolds numbers, accelerations, and history effects. Unlike previous models that solely apply to standard flows, the present framework reconciles nonstandard flows with standard flows and enables accurate estimates of wall friction in numerical simulations and experiments without resolving the viscous sublayer or using the law of the wall.

DOI: 10.1103/PhysRevLett.132.014001

Introduction.—Fluids flowing adjacent to solid surfaces experience a resisting force due to friction between the flow and the surface. This surface friction (also referred to as wall friction) depends on the character of the flow, namely, laminar, transitional or turbulent, which in turn depends on the flow Reynolds number Re (to be defined later). Most flows of practical relevance have high Reynolds numbers and are therefore, turbulent. In order to maintain a turbulent flow, energy needs to be supplied to overcome the work of wall friction; a reference frame wherein the wall moves upstream and fluid far away is stationary, is convenient to visualize the work of wall friction [1]. Therefore, wall friction dictates economics of flow processes such as the pumping power required to push fluids through pipe lines, consumption of aviation fuel by commercial airliners, and so on [2–5]. Hydrodynamically, rough walls cause more friction compared to smooth ones [6,7]. Thus, surfaces in most applications are polished or coated to be smooth to reduce operating costs. Even then, friction at these smooth walls contributes a major chunk of the financial burden passed on to the end users. Friction scaling and predictive models in smooth-wall turbulence have therefore been intensely studied for over a century [6,8–15], and are the focus of this Letter as well.

Smooth-wall turbulent flows may be classified as internal flows (fully developed pipe and channel flows) and external flows (boundary layers). Turbulent boundary layers (TBLs) are of three broad types: (a) no acceleration of the freestream, i.e., freestream velocity $U_\infty =$ constant due to the pressure-gradient force being zero (ZPG TBLs), (b) decelerating freestream, i.e., U_∞ is a decreasing function of the streamwise coordinate x due to adverse (opposing the flow) pressure gradient force (APG TBLs), and (c) accelerating freestream, i.e., U_∞ is an increasing function of x due to favorable (assisting the flow) pressure gradient force (FPG TBLs). For a very strong APG, the boundary layer may start "approaching" separation so that, wall friction no longer remains dynamically relevant [2]. Our study therefore, comprises of internal flows, and all "attached" TBLs (Fig. 1) which also include, for the first time as far as we know, (i) a wide variety of non-self-similar TBLs, such as those over aircraft wings and turbine blades, and (ii) compressible (supersonic and

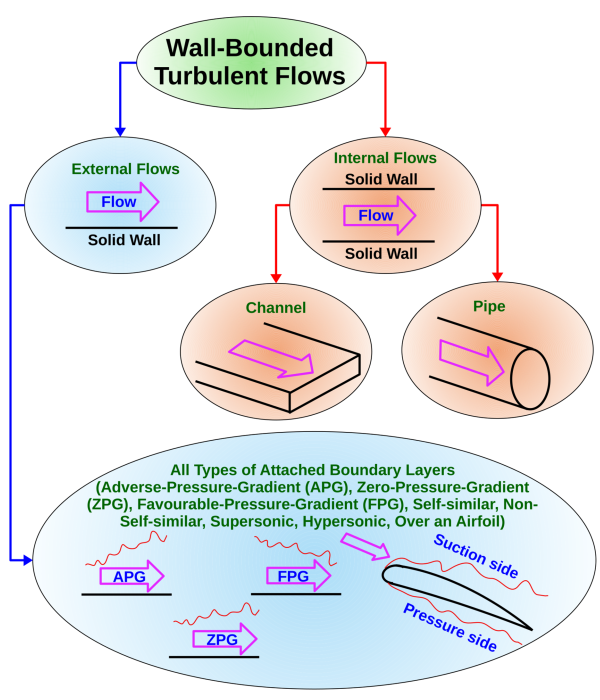

FIG. 1. Smooth-wall turbulent flows covered by this study. All flows are two dimensional in the mean. Internal flows are fully developed. External flows are different types of attached TBLs. Thick black lines indicate solid wall(s) and arrows indicate nominal flow direction. Thin red lines schematically indicate turbulent-nonturbulent interface, a measure of the thickness of TBLs.

hypersonic) TBLs with Van-Driest-transformed mean velocity profiles [16–19].

Drawbacks of existing scalings and models.—All friction scalings and models are mathematical descriptions of how a dimensionless measure f of friction varies with flow Reynolds number Re [9,11,14,15,20], where f and Re are defined by

$$f \coloneqq \sqrt{\tau/\rho U_s^2} = U_\tau/U_s \quad \text{and} \quad \mathrm{Re} \coloneqq \delta U_s/\nu. \tag{1}$$

Here, ρ is the density of flowing fluid, τ is the shear stress between the flow and the wall, $U_\tau \coloneqq \sqrt{\tau/\rho}$ is the friction velocity (throughout this Letter, $\coloneqq$ denotes a definition), δ is the outer length scale of the flow (boundary layer height or pipe radius or channel half-height), and ν is the kinematic viscosity of the fluid. The velocity scale U_s should (i) render τ (or U_τ) and δ dimensionless, and (ii) "scale" the data in a universal fashion in (f, Re) coordinates.

Despite the extensive research taken place so far, all f-Re relations in the literature suffer from two major shortcomings.

(1) From a fundamental point of view, these relations are not founded firmly in the governing dynamics of turbulent flows. Mostly, they are by-products of mean velocity scaling laws which themselves, are physically intuitive but still empirical. Specifically, it is a tradition to use U_∞ (freestream velocity for TBLs and center-line or bulk velocity for pipes and channels) as the velocity scale ($U_s = U_\infty$) in Eq. (1). However, this is simply because U_∞ is either specified as the outer velocity boundary condition (BC) in TBLs or is a practically useful measure of flow rate through pipe or channel. There is no "dynamical" basis for setting $U_s = U_\infty$; (2) From a practical point of view, the applicability of these relations is too restrictive, limited to only certain types of flows studied extensively using experiments and numerical simulations. These "standard" flows are ZPG TBLs, and fully-developed pipe and channel flows. Most practical flows of interest are, however, "nonstandard" and departures from the standard behavior are significant. These include self-similar and non-self-similar TBLs in strong APGs and FPGs, and compressible TBLs. For example, a TBL developing over an aircraft wing or turbine blade experiences strong PG that also varies in the streamwise direction much more rapidly compared to the intrinsic timescale of turbulence adjustments [21], and this mismatch renders these flows non-self-similar. Individual f-Re relations cannot be devised for such flows due to the diversity of flow situations that could arise. The generalized universal f-Re framework, which is the focus of this Letter, offers an elegant solution to this problem.

To highlight these issues, we consider friction data from several types of flows shown in Fig. 1. These data come from experiments and numerical simulation studies

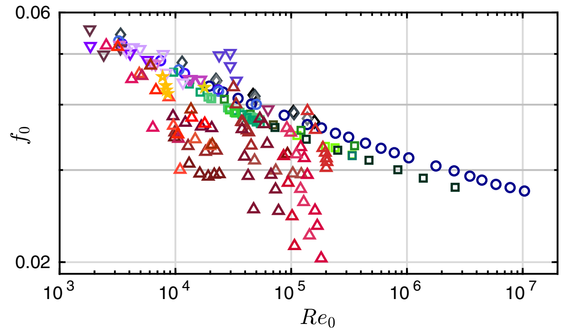

FIG. 2. Traditional scaling of friction ($f_0 \coloneqq U_\tau/U_\infty$ and $\mathrm{Re}_0 \coloneqq \delta U_\infty/\nu$) in smooth-wall turbulent flows. Circles—pipes, squares—ZPG TBLs, diamonds—channels, triangles—APG TBLs (self-similar and non-self-similar), inverted triangles—FPG TBLs (self-similar and non-self-similar), and pentacles—compressible TBLs. Further details of symbols and datasets are in Supplemental Material Part IIC—Data Tables [22]. Data cover Reynolds number range $95 \le \mathrm{Re}_\tau \le 528\,860$ (more than three decades in Re_τ) and dimensionless pressure gradient range $-1.5 \le \beta \le 35.9$ (from strong FPG to strong APG). Note that, $\mathrm{Re}_\tau \coloneqq \delta U_\tau/\nu$ is the friction Reynolds number and $\beta \coloneqq \delta^*/\tau(dp/dx)$ is the Rotta-Clauser pressure gradient parameter [62,63]; δ^* is displacement thickness and dp/dx is mean streamwise pressure gradient.

published in the literature, and cover very wide ranges of Reynolds number and PG (Supplemental Material Part IIC—Data Tables [22]). Figure 2 plots friction data in the traditional scaling framework (f_0, Re_0) where $f_0 \coloneqq U_\tau/U_\infty$ and $\mathrm{Re}_0 \coloneqq \delta U_\infty/\nu$, i.e., $U_s = U_\infty$ in Eq. (1). Different datasets show very different trends as well as varying degrees of scatter. Figure 2 clearly demonstrates the absence of any generalized scaling behavior in the (f_0, Re_0) framework, precluding any possibility of making useful predictions.

Physical basis for generalized scaling.—Fundamentally, the velocity field of every turbulent flow is a solution of the governing dynamical equations subject to certain initial and boundary conditions (ICs and BCs). For statistically stationary flows, only BCs are relevant; all flows considered here are statistically stationary. Friction at the wall is a consequence of the no-slip BC at the wall and is related to the gradient of mean velocity field in the vicinity of the wall. This region receives velocity contributions from turbulent motions or eddies that span a wide range of scales. The smallest eddies are dissipative and have sizes of the order of Kolmogorov length scale; the largest eddies are energetic and scale on δ [2,3]. Further, large eddies organize in the form of large-scale motions (LSMs) [64,65], and very-large-scale motions (VLSMs) in internal flows [66] or superstructures in external flows [67,68]. This rich spectral structure of a turbulence cascade is set up by nonlinearity of governing Naviér-Stokes equations through vortex stretching mechanism [2]. Since friction at the wall receives contributions from this entire spectrum of scales [69–73], a meaningful "scaling" of friction must follow from the flow

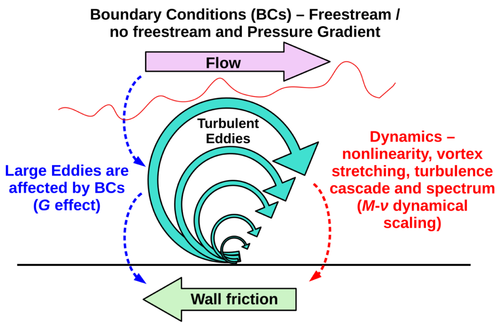

FIG. 3. Schematic depicting roles of dynamics and BCs towards setting up and modulating eddies of turbulence that contribute to friction experienced by the flow at the wall. Dynamics contributes M-ν scaling and effects of BCs are taken into account by Clauser's shape factor G, both together yielding generalized M-ν-G scaling.

dynamics that embodies this structure of turbulence. It is important to note that, BCs are not central to setting up the eddy cascade. They are, however, peripherally important since they modulate the strength of large eddies in a manner that differs from one type of flow to another [74,75]. Therefore, BCs could influence friction at the wall in an indirect fashion through their influence on the large eddies. With this physical insight, it is clear that the quest for a generalized scaling of friction, valid for all flows, must take into cognizance both, the dynamics and the BCs as illustrated schematically in Fig. 3. Note that, the traditional choice of velocity scale $U_s = U_\infty$ mentioned earlier, completely misses the dynamics since U_∞ is technically just the outer velocity BC.

Unified scaling in standard flows.—Our recent work [20] presents analysis of friction scaling in standard flows (ZPG TBLs, pipes and channels) along the lines discussed above. It shows how dynamics and BCs can be used to unify the scaling of friction in these flows. The analysis consists of two parts. First, the equation governing the evolution of streamwise mean-flow kinetic energy $U^2/2$ is considered in its wall-normally integrated form; this step bears striking resemblance to the approach of Renard and Deck [1] who decompose wall friction into contributions from physical phenomena across the complete TBL. The asymptotic form of this equation shows that the dynamics sets its own velocity scale for friction [20]. This new dynamical velocity scale is different from U_∞, and is given by M/ν where $M = \int_0^\delta U^2 dz$ is proportional to total streamwise kinetic energy content of the mean flow. With $U_s = M/\nu$ in Eq. (1), dimensionless friction and the Reynolds number become

$$f_1' := U_\tau \nu / M \quad \text{and} \quad \mathrm{Re}_1' := \delta M/\nu^2. \tag{2}$$

This nondimensionalization is referred to as M-ν scaling of friction and is founded firmly on the dynamics of wall-bounded turbulent shear flows. All standard flows are shown to obey the dynamical asymptotic friction scaling law $f_1' \sim \mathrm{Re}_1'^{-1/2}$ in the limit of an infinite Reynolds number. For a given finite-Re standard flow, friction in M-ν scaling may be treated as a small perturbation from the asymptotic scaling law. Using asymptotic series expansions, a finite-Re model in the M-ν scaling framework is obtained [14,20]. This model combines contributions to friction from inviscid attached-eddy-type motions as well as small-scale, dissipative motions that are not captured by the attached-eddy model (Supplemental Material Part IB [22]). The model very well describes variation of f_1' with Re_1' for each individual standard flow type, but fails when all of them are taken together [20]. This happens because M-ν scaling does not account for any BC effects; at finite Reynolds numbers, BCs for different standard flows are different [20]. The second part of the analysis proposes that the shape of the mean velocity profile is a useful measure of the distinguishing effects of BCs. Empirical transformations are proposed [20] to obtain "effective" dimensionless friction f_1 and Reynolds number Re_1 where shape of mean velocity profile has been factored in. These transformations are

$$f_1 = f_1'(G/G_{\mathrm{ref}})^p \quad \text{and} \quad \mathrm{Re}_1 = \mathrm{Re}_1'(G/G_{\mathrm{ref}})^q, \tag{3}$$

where G is Clauser's shape factor [76], for the outer-scaled or defect velocity profile, defined as $G := U_\infty/U_\tau[(H-1)/H]$ wherein H is the conventional shape factor ($H := \delta^*/\theta$ where δ^* is displacement thickness and θ is momentum thickness), $G_{\mathrm{ref}} = 6.8$ is the reference value of G corresponding to the ZPG TBL at high Reynolds number [20,76], and p and q are empirical (constant) exponents. Thus, $(G/G_{\mathrm{ref}})^p$ and $(G/G_{\mathrm{ref}})^q$ in Eq. (3) are empirical top ups, on the basic dynamical scaling of friction [Eq. (2)], accounting for BC effects. This scaling framework of coordinates (f_1, Re_1) is termed as M-ν-G scaling (Supplemental Material Part I [22]). The finite-Re friction model (M-ν-G scaling) unifying friction in standard flows [20] is

$$f_1 = \frac{A_1}{\ln \mathrm{Re}_1} \mathrm{Re}_1^{\left[B_0 + \frac{B_1}{\sqrt{\ln \mathrm{Re}_1}}\right]}. \tag{4}$$

Model coefficients A_1, B_0, B_1, and empirical (constant) transformation exponents p and q are determined by optimizing the fit of Eq. (4) to the data (Supplemental Material Part II-A [22]). Friction data from all standard flows are described very well, in a unified manner, by the M-ν-G scaling [Eq. (3)] and finite-Re model Eq. (4) [20].

Hypothesis of generalized scaling in all flows.—We now hypothesize that the M-ν-G scaling and friction model [Eq. (4)] are generally applicable to all flows. For this to happen, the following three conditions need to be satisfied: (i) M-ν scaling should apply to all flows, (ii) nonstandard flows can have strong PGs and mathematically, PG is a BC. Therefore, G, which accounts for BC effects in standard flows, should account for strong PG effects in nonstandard flows, and (iii) nonstandard flows can have strong streamwise variations in PG giving rise to PG history or memory effects, and G should also account for these effects.

With reference to the first condition, we note that a cornerstone assumption for M-ν scaling in standard flows [20] is the turbulence kinetic energy (TKE) production term in the log-law-type overlap varying inversely with distance from the wall, i.e., $P_{+,\mathrm{overlap}} \sim 1/z_+$; $z_+ \coloneqq zU_\tau/\nu$ is the distance from the wall in viscous units. For nonstandard flows, the extent, slope and intercept of the log region vary with PG strength [77–81]. Alternatively, there are proposals arguing in favor of power-law-type overlap. If the type of overlap (log-law-type or power-law-type) is not specified, then the variation of production term may be generally written as $P_{+,\mathrm{overlap}} \sim 1/z_+^m$ $(m > 0)$; $m = 1$ corresponds to log-law-type overlap. Supplemental Material Part I [22] provides derivations of M-ν scaling for all possible overlaps $m = 1$, $0 < m < 1$ and $m > 1$. These derivations are new and account for the region below the overlap layer (viscous sublayer, buffer layer and mesolayer) in addition to overlap and wake layer regions. In all cases, the dynamics dictates the same M-ν scaling irrespective of the type of overlap and wall-normal extents of various flow regions. Therefore, the first condition mentioned above is satisfied for all flows. As to the second condition, it is known that G is a function of dimensionless PG in case of self-similar TBLs [62,82]. Therefore, one may readily expect G to capture strong PG effects, satisfying the second condition. Finally, flows with rapid variations of dimensionless PG are inevitably characterized by strong history effects wherein wall-normal distributions of turbulent stresses do not scale simply on local variables (self-similarity fails), but depend strongly on the upstream distribution of PG the flow has experienced [83]. This memory is due to large-scale structures such as LSMs and VLSMs or superstructures, that take longer time to adjust to the BCs compared to the timescale of the variation of PG BC itself [21]. As such, streamwise distributions of the Reynolds number, skin friction coefficient ($C_f \coloneqq 2f_0^2$), conventional shape factor (H), etc. lag behind the streamwise variation of dimensionless PG [80,84,85]. However, careful scrutiny reveals that the streamwise variations of C_f and H follow each other very well albeit with opposite phases; H increases (decreases) with C_f decrease (increase). This is evident in several studies [Fig. 5(b) of Fernholz and Warnack [84], Figs. 3 and 4 of Warnack and Fernholz [85], Fig. 3 and Table 1 of Aubertine and Eaton [86], Fig. 6 of Bourassa and Thomas [80], Fig. 4 of Vinuesa *et al.* [87], Fig. 5 of Bobke *et al.* [83], Figs. 1(b) and 1(d) of Maciel *et al.* [63], Fig. 3 of Dróżdż *et al.* [88]]. Since G is related to H and C_f [76], its variation is also in tune with that of H or C_f [Figs. 1(b), 1(d), and 1(e) of Maciel *et al.* [63]]. Most importantly, Figs. 2(a), 3, 6, and 7 of Bobke *et al.* [83] reveal that for matched local values of dimensionless PG and Reynolds number, the shapes of viscous-scaled mean velocity profiles differ (G values are different) depending on the PG history. Further, it has been suggested in the literature that H captures history effects in TBLs [63,88,89]. Taken together, the empirical evidence indeed suggests that G could capture PG history effects as well. This satisfies the third condition. In view of these facts, one may expect M-ν-G scaling Eq. (3) and friction model Eq. (4) to hold generally for all flows (Supplemental Material Part I [22]).

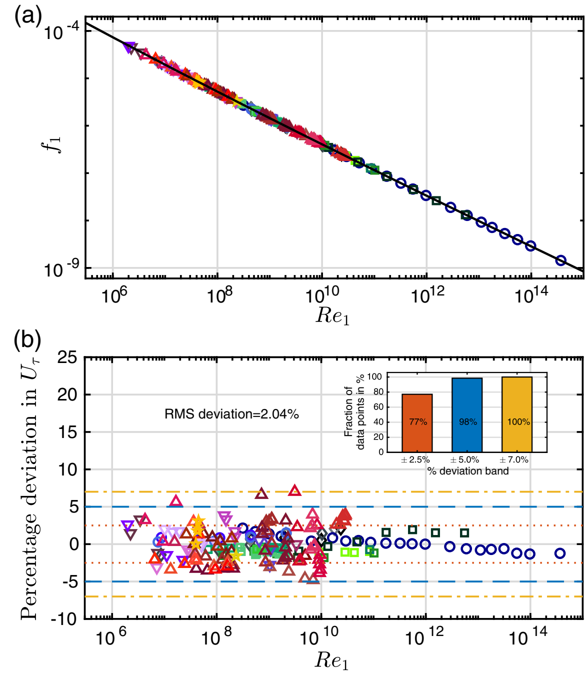

FIG. 4. (a) Generalized universal M-ν-G scaling of friction in smooth-wall turbulent flows. Solid line shows generalized finite-Re friction model Eq. (4) fitted to all data. (b) Percentage deviation of predicted U_τ from its actual value. Dotted, dashed, and dashed-dotted horizontal lines, respectively, indicate deviation bands of ±2.5%, ±5%, and ±7%. Inset shows histogram of the fraction of data points contained in these bands. For symbols, see caption of Fig. 2.

Hypothesis testing.—To test our hypothesis, we process and plot all data in M-ν-G scaling [Fig. 4(a)]. Friction model Eq. (4) fitted to the data is also plotted. Data processing is outlined in Supplemental Material Part IIA [22]. The model coefficients are $A_1 = 2.0699$, $B_0 = -0.4749$ and $B_1 = -0.2860$ [Eq. (4)], and empirical exponents are $p = 0.5392$ and $q = -0.5451$ [Eq. (3)]. Data in Fig. 4(a) tightly cluster around the fitted friction model [Eq. (4)] which can now be used to predict U_τ in any flow. Prediction involves solving implicit Eq. (4)—U_τ occurs on both sides due to the presence of G in f_1 and Re_1 [Eq. (3)]—using measured or computed velocity profile data (Supplemental Material Part IIB [22]); viscous sublayer data or law-of-the-wall assumptions are not required (Supplemental Material Part III [22]). Figure 4(b) plots, for all data points, the percentage deviation of the predicted value of U_τ from the actual value in measurements or simulations. An impressive root-mean-squared (RMS) deviation of 2.04% is evident with a $\pm 5\%$ band covering almost all the deviations. Note that, 85 data points out of the total 192 correspond to standard flows and the remaining 107 correspond to nonstandard flows that involve strong PGs and/or PG history effects. Results are therefore not biased by standard flows. While dedicated models tailored to individual flows could achieve better prediction accuracy, results of Fig. 4 unequivocally confirm that our hypothesis stands scrutiny of the data, and our generalized M-ν-G scaling [Eq. (3)] and friction model [Eq. (4)] show high fidelity in handling wide variety of flows over very broad ranges of Reynolds number, PG and PG history effects.

Conclusion.—High-Re, nonstandard flows such as those over wings and fuselage of an aircraft or the nose and body of launch vehicles and missiles, are of great importance to practising designers and engineers. Standard flows, on the other hand, are mainly of interest to academicians as systematic tools for unveiling the behavior of wall turbulence. Strong PG and PG history effects make nonstandard flows hard to predict. The present results, for the first time, show that our generalized scaling and model for friction, founded firmly on the dynamics and BCs, and supported strongly by data from experiments and simulations, bring out an inherent universality of friction in all attached, smooth-wall turbulent flows. The results are very relevant to both modelers and experimentalists. For estimating wall friction, the viscous sublayer next to the wall needs to be resolved [90] which is computationally expensive or experimentally formidable [91] in high-Re flows. Alternatively, wall functions (based on the law of the wall) may be used if the first resolved (or measured) point is beyond the viscous sublayer [92,93]. For nonstandard flows, however, the law of the wall is not universal [78,93]. Our generalized friction model shows promising potential to accurately estimate wall friction in numerical simulations and experiments of high-Re, nonstandard flows without resolving the viscous sublayer or relying on the law of the wall.

We thank Director, IITM for continued support to the Fluid Dynamics Laboratory. IITM is an autonomous research institute under Ministry of Earth Sciences (MoES), Government of India. Thanks are also due to researchers for sharing data that are used in this work.

[*]sadixit@tropmet.res.in

[1] N. Renard and S. Deck, A theoretical decomposition of mean skin friction generation into physical phenomena across the boundary layer, J. Fluid Mech. **790**, 339 (2016).

[2] H. Tennekes and J. L. Lumley, *A First Course in Turbulence* (MIT Press, Cambridge, MA, 1972).

[3] P. A. Davidson, *Turbulence: An Introduction for Scientists and Engineers*, 2nd ed. (Oxford University Press, New York, 2015).

[4] B. J. McKeon, Controlling turbulence, Science **327**, 1462 (2010).

[5] I. Marusic, R. Mathis, and N. Hutchins, Predictive model for wall-bounded turbulent flow, Science **329**, 193 (2010).

[6] J. Nikuradse, *Strömungsgesetze in Rauhen Rohren*, VDI-Forschungsheft 361. Beilage-zu "Forschung auf dem Gebiete des Ingenieurwesens" Ausgabe B Band 4 (1933).

[7] G. Gioia and P. Chakraborty, Turbulent friction in rough pipes and the energy spectrum of the phenomenological theory, Phys. Rev. Lett. **96**, 044502 (2006).

[8] L. Prandtl, *Über Flüssigkeitsbewegung bei sehr kleiner Reibung, Verhandlungen des dritten internationalen Mathematiker-Kongresses* (Heidelberg, Leipzig, 1904), pp. 489–491 [On the motion of fluids with very little friction, in *Early Developments of Modern Aerodynamics*, edited by (Butterworth-Heinemann, Oxford, 2001, 1904), pp. 77–84].

[9] H. H. Fernholz and P. J. Finley, The incompressible zero-pressure-gradient turbulent boundary layer: An assessment of the data, Prog. Aerosp. Sci. **32**, 245 (1996).

[10] B. J. McKeon, C. J. Swanson, M. V. Zagarola, R. J. Donnelly, and A. J. Smits, Friction factors for smooth pipe flow, J. Fluid Mech. **511**, 41 (2004).

[11] B. J. McKeon, M. V. Zagarola, and A. J. Smits, A new friction factor relationship for fully developed pipe flow, J. Fluid Mech. **538**, 429 (2005).

[12] E.-S. Zanoun, F. Durst, O. Bayoumy, and A. Al-Salaymeh, Wall skin friction and mean velocity profiles of fully developed turbulent pipe flows, Exp. Therm. Fluid. Sci. **32**, 249 (2007).

[13] E.-S. Zanoun, H. Nagib, and F. Durst, Refined C_f relation for turbulent channels and consequences for high-Re experiments, Fluid Dyn. Res. **41**, 021405 (2009).

[14] S. A. Dixit, A. Gupta, H. Choudhary, A. K. Singh, and T. Prabhakaran, Asymptotic scaling of drag in flat-plate turbulent boundary layers, Phy. Fluids **32**, 041702 (2020).

[15] S. A. Dixit, A. Gupta, H. Choudhary, A. K. Singh, and T. Prabhakaran, A new universal model for friction factor in smooth pipes, Phys. Fluids **33**, 035134 (2021).

[16] S. Pirozzoli, F. Grasso, and T. B. Gatski, Direct numerical simulation and analysis of a spatially evolving supersonic turbulent boundary layer at $M = 2.25$, Phys. Fluids **16**, 530 (2004).

[17] A. J. Smits and J.-P. Dussauge, *Turbulent Shear Layers in Supersonic Flow* (Springer Science & Business Media, New York, 2006).

[18] M. P. Martin, Direct numerical simulation of hypersonic turbulent boundary layers. Part 1. Initialization and comparison with experiments, J. Fluid Mech. **570**, 347 (2007).

[19] S. Pirozzoli and M. Bernardini, Turbulence in supersonic boundary layers at moderate Reynolds number, J. Fluid Mech. **688**, 120 (2011).

[20] S. A. Dixit, A. Gupta, H. Choudhary, and T. Prabhakaran, Universal scaling of mean skin friction in turbulent boundary layers and fully developed pipe and channel flows, J. Fluid Mech. **943**, 1 (2022).

[21] W. J. Devenport and K. T. Lowe, Equilibrium and non-equilibrium turbulent boundary layers, Prog. Aerosp. Sci. **131**, 100807 (2022).

[22] See Supplemental Material at http://link.aps.org/supplemental/10.1103/PhysRevLett.132.014001 for detailed derivations, data selection and processing details, data tables, and additional sensitivity analysis for unavailability of near-wall data. The Supplemental Material includes additional references listed here as Refs. [23–61].

[23] D. B. Spalding, A single formula for the law of the wall, J. Appl. Mech. **28**, 455 (1961).

[24] G. I. Barenblatt, Scaling laws for fully developed turbulent shear flows. Part 1. Basic hypotheses and analysis, J. Fluid Mech. **248**, 513 (1993).

[25] G. I. Barenblatt, A. J. Chorin, and V. M. Prostokishin, Scaling laws for fully developed turbulent flow in pipes, Appl. Mech. Rev. **50**, 413 (1997).

[26] W. K. George and L. Castillo, Zero-pressure-gradient turbulent boundary layer, Appl. Mech. Rev. **50**, 689 (1997).

[27] N. Afzal, Power law and log law velocity profiles in turbulent boundary-layer flow: Equivalent relations at large Reynolds numbers, Acta Mech. **151**, 195 (2001).

[28] N. Afzal, A. Seena, and A. Bushra, Power law velocity profile in fully developed turbulent pipe and channel flows, J. Hydraul. Eng. **133**, 1080 (2007).

[29] A. J. Smits, B. J. McKeon, and I. Marusic, High–Reynolds number wall turbulence, Annu. Rev. Fluid Mech. **43** (2011).

[30] I. Marusic, J. P. Monty, M. Hultmark, and A. J. Smits, On the logarithmic region in wall turbulence, J. Fluid Mech. **716**, R3 (2013).

[31] K. R. Sreenivasan and A. Sahay, The persistence of viscous effects in the overlap region, and the mean velocity in turbulent pipe and channel flows, in *In Self-Sustaining Mechanisms of Wall Turbulence*, edited by R. Panton (Computational Mechanics Publications, Southampton, 1997), pp. 253–272.

[32] S. A. Dixit and O. N. Ramesh, Streamwise self-similarity and log scaling in turbulent boundary layers, J. Fluid Mech. **851**, R1 (2018).

[33] R. Narasimha and K. R. Sreenivasan, Relaminarization in highly accelerated turbulent boundary layers, J. Fluid Mech. **61**, 417 (1973).

[34] P. G. Huang, G. N. Coleman, and P. Bradshaw, Compressible turbulent channel flows: DNS results and modelling, J. Fluid Mech. **305**, 185 (1995).

[35] H. Foysi, S. Sarkar, and R. Friedrich, Compressibility effects and turbulence scalings in supersonic channel flow, J. Fluid Mech. **509**, 207 (2004).

[36] D. Modesti and S. Pirozzoli, Reynolds and Mach number effects in compressible turbulent channel flow, Int. J. Heat Fluid Flow **59**, 33 (2016).

[37] P. S. Volpiani, P. S. Iyer, S. Pirozzoli, and J. Larsson, Data-driven compressibility transformation for turbulent wall layers, Phys. Rev. Fluids **5**, 052602(R) (2020).

[38] P. Dengel and H. H. Fernholz, An experimental investigation of an incompressible turbulent boundary layer in the vicinity of separation, J. Fluid Mech. **212**, 615 (1990).

[39] M. P. Schultz and K. A. Flack, Reynolds-number scaling of turbulent channel flow, Phys. Fluids **25**, 025104 (2013).

[40] M. Bernardini, S. Pirozzoli, and P. Orlandi, Velocity statistics in turbulent channel flow up to $\mathrm{Re}_\tau \approx 4000$, J. Fluid Mech. **742**, 171 (2014).

[41] M. Lee and R. D. Moser, Direct numerical simulation of turbulent channel flow up to $\mathrm{Re}_\tau \approx 5200$, J. Fluid Mech. **774**, 395 (2015).

[42] M. V. Zagarola and A. J. Smits, Mean-flow scaling of turbulent pipe flow, J. Fluid Mech. **373**, 33 (1998).

[43] B. J. Mckeon, J. Li, W. Jiang, J. F. Morrison, and A. J. Smits, Further observations on the mean velocity distribution in fully developed pipe flow, J. Fluid Mech. **501**, 135 (2004).

[44] G. K. El Khoury, P. Schlatter, A. Noorani, P. F. Fischer, G. Brethouwer, and A. V. Johansson, Direct numerical simulation of turbulent pipe flow at moderately high Reynolds numbers, Flow Turbul. Combust. **91**, 475 (2013).

[45] C. Chin, J. P. Monty, and A. Ooi, Reynolds number effects in DNS of pipe flow and comparison with channels and boundary layers, Int. J. Heat Fluid Flow **45**, 33 (2014).

[46] I. Marusic, K. A. Chauhan, V. Kulandaivelu, and N. Hutchins, Evolution of zero-pressure-gradient boundary layers from different tripping conditions, J. Fluid Mech. **783**, 379 (2015).

[47] K. M. Talluru, R. Baidya, N. Hutchins, and I. Marusic, Amplitude modulation of all three velocity components in turbulent boundary layers, J. Fluid Mech. **746** (2014).

[48] D. B. DeGraaff and J. K. Eaton, Reynolds-number scaling of the flat-plate turbulent boundary layer, J. Fluid Mech. **422**, 319 (2000).

[49] R. Örlü and P. Schlatter, Comparison of experiments and simulations for zero pressure gradient turbulent boundary layers at moderate Reynolds numbers, Exp. Fluids **54**, 1 (2013).

[50] J. Jiménez, S. Hoyas, M. P. Simens, and Y. Mizuno, Turbulent boundary layers and channels at moderate Reynolds numbers, J. Fluid Mech. **657**, 335 (2010).

[51] J. A. Sillero, J. Jiménez, and R. D. Moser, One-point statistics for turbulent wall-bounded flows at Reynolds numbers up to $\delta_+ \approx 2000$, Phys. Fluids **25**, 105102 (2013).

[52] P. Schlatter and R. Örlü, Assessment of direct numerical simulation data of turbulent boundary layers, J. Fluid Mech. **659**, 116 (2010).

[53] P. R. Spalart, Numerical study of sink-flow boundary layers, J. Fluid Mech. **172**, 307 (1986).

[54] R. Vinuesa, P. S. Negi, M. Atzori, A. Hanifi, D. S. Henningson, and P. Schlatter, Turbulent boundary layers around wing sections up to $\mathrm{Re}_c = 1{,}000{,}000$, Int. J. Heat. Fluid Flow **72**, 86 (2018).

[55] J. P. Monty, Z. Harun, and I. Marusic, A parametric study of adverse pressure gradient turbulent boundary layers, Int. J. Heat. Fluid Flow **32**, 575 (2011).

[56] M. Skote, D. S. Henningson, and R. A. W. M. Henkes, Direct numerical simulation of self-similar turbulent boundary layers in adverse pressure gradients, Flow Turbul. Combust. **60**, 47 (1998).

[57] C. D. Aubertine, Reynolds number effects on an adverse pressure gradient turbulent boundary layer, Ph.D. thesis, 2005.

[58] A. Dróżdż and W. Elsner, An experimental study of turbulent boundary layers approaching separation, Int. J. Heat. Fluid Flow **68**, 337 (2017).

[59] N. Hutchins and K.-S. Choi, Accurate measurements of local skin friction coefficient using hot-wire anemometry, Prog. Aerosp. Sci. **38**, 421 (2002).

[60] F. M. White, *Viscous Fluid Flow*, 2nd ed. (McGraw-Hill Inc., New York, 1991).

[61] P. A. Monkewitz, K. A. Chauhan, and H. M. Nagib, Self-consistent high-Reynolds-number asymptotics for zero-pressure-gradient turbulent boundary layers, Phys. Fluids **19** (2007).

[62] F. H. Clauser, Turbulent boundary layers in adverse pressure gradients, J. Aero. Sci. **21**, 91 (1954).

[63] Y. Maciel, T. Wei, A. G. Gungor, and M. P. Simens, Outer scales and parameters of adverse-pressure-gradient turbulent boundary layers, J. Fluid Mech. **844**, 5 (2018).

[64] R. J. Adrian, C. D. Meinhart, and C. D. Tomkins, Vortex organization in the outer region of the turbulent boundary layer, J. Fluid Mech. **422**, 1 (2000).

[65] K. T. Christensen and R. J. Adrian, Statistical evidence of hairpin vortex packets in wall turbulence, J. Fluid Mech. **431**, 433 (2001).

[66] K. C. Kim and R. J. Adrian, Very large-scale motion in the outer layer, Phys. Fluids **11**, 417 (1999).

[67] N. Hutchins and I. Marusic, Large-scale influences in near-wall turbulence, Phil. Trans. R. Soc. A **365**, 647 (2007).

[68] N. Hutchins and I. Marusic, Evidence of very long meandering features in the logarithmic region of turbulent boundary layers, J. Fluid Mech. **579**, 1 (2007).

[69] K. Fukagata, K. Iwamoto, and N. Kasagi, Contribution of Reynolds stress distribution to the skin friction in wall-bounded flows, Phys. Fluids **14**, L73 (2002).

[70] S. Deck, N. Renard, R. Laraufie, and P.-É. Weiss, Large-scale contribution to mean wall shear stress in high-Reynolds-number flat-plate boundary layers up to $\mathrm{Re}_\theta = 13650$, J. Fluid Mech. **743**, 202 (2014).

[71] M. D. Giovanetti, Y. Hwang, and H. Choi, Skin-friction generation by attached eddies in turbulent channel flow, J. Fluid Mech. **808**, 511 (2016).

[72] J. Hwang and H. J. Sung, Influence of large-scale motions on the frictional drag in a turbulent boundary layer, J. Fluid Mech. **829**, 751 (2017).

[73] Y. Fan, C. Cheng, and W. Li, Effects of the Reynolds number on the mean skin friction decomposition in turbulent channel flows, Appl. Math. Mech. **40**, 331 (2019).

[74] J. P. Monty, N. Hutchins, H. C. H. Ng, I. Marusic, and M. S. Chong, A comparison of turbulent pipe, channel and boundary layer flows, J. Fluid Mech. **632**, 431 (2009).

[75] H. Zambri, J. P. Monty, R. Mathis, and I. Marusic, Pressure gradient effects on the large-scale structure of turbulent boundary layers, J. Fluid Mech. **715**, 477 (2013).

[76] F. H. Clauser, The turbulent boundary layer, in *Advances in Applied Mechanics* (Elsevier, New York, 1956), Vol. 4, pp. 1–51.

[77] T. B. Nickels, Inner scaling for wall-bounded flows subject to large pressure gradients, J. Fluid Mech. **521**, 217 (2004).

[78] K. A. Chauhan, H. M. Nagib, and P. A. Monkewitz, Evidence on non-universality of Kármán constant, in *Proceedings of iTi Conference in Turbulence 2005, Springer Proceedings in Physics, Progress in Turbulence* (Springer-Verlag, Berlin Heidelberg, 2007), Vol. II, pp. 159–163.

[79] S. A. Dixit and O. N. Ramesh, Pressure-gradient-dependent logarithmic laws in sink flow turbulent boundary layers, J. Fluid Mech. **615**, 445 (2008).

[80] C. Bourassa and F. O. Thomas, An experimental investigation of a highly accelerated turbulent boundary layer, J. Fluid Mech. **634**, 359 (2009).

[81] J. H. Lee, Large-scale motions in turbulent boundary layers subjected to adverse pressure gradients, J. Fluid Mech. **810**, 323 (2017).

[82] G. L. Mellor and D. M. Gibson, Equilibrium turbulent boundary layers, J. Fluid Mech. **24**, 225 (1966).

[83] A. Bobke, R. Vinuesa, R. Örlü, and P. Schlatter, History effects and near equilibrium in adverse-pressure-gradient turbulent boundary layers, J. Fluid Mech. **820**, 667 (2017).

[84] H. H. Fernholz and D. Warnack, The effects of a favourable pressure gradient and of the Reynolds number on an incompressible axisymmetric turbulent boundary layer. Part 1. The turbulent boundary layer, J. Fluid Mech. **359**, 329 (1998).

[85] D. Warnack and H. H. Fernholz, The effects of a favourable pressure gradient and of the Reynolds number on an incompressible axisymmetric turbulent boundary layer. Part 2. The boundary layer with relaminarization, J. Fluid Mech. **359**, 357 (1998).

[86] C. D. Aubertine and J. K. Eaton, Turbulence development in a non-equilibrium turbulent boundary layer with mild adverse pressure gradient, J. Fluid Mech. **532**, 345 (2005).

[87] R. Vinuesa, S. M. Hosseini, A. Hanifi, D. S. Henningson, and P. Schlatter, Pressure-gradient turbulent boundary layers developing around a wing section, Flow Turbul. Combust. **99**, 613 (2017).

[88] A. Dróżdż, P. Niegodajew, M. Romańczyk, and W. Elsner, Effect of Reynolds number on turbulent boundary layer approaching separation, Exp. Therm. Fluid. Sci. **125**, 110377 (2021).

[89] A. Dróżdż, W. Elsner, P. Niegodajew, R. Vinuesa, R. Örlü, and P. Schlatter, A description of turbulence intensity profiles for boundary layers with adverse pressure gradient, Eur. J. Mech. B **84**, 470 (2020).

[90] J. H. Ferziger, M. Perić, and R. L. Street, *Computational Methods for Fluid Dynamics* (springer, New York, 2019).

[91] M. Vallikivi, M. Hultmark, and A. J. Smits, Turbulent boundary layer statistics at very high Reynolds number, J. Fluid Mech. **779**, 371 (2015).

[92] T. Knopp, T. Alrutz, and D. Schwamborn, A grid and flow adaptive wall-function method for RANS turbulence modelling, J. Comput. Phys. **220**, 19 (2006).

[93] T. Knopp, An empirical wall law for the mean velocity in an adverse pressure gradient for RANS turbulence modelling, Flow Turbul. Combust. **109**, 571 (2022).